Journal of Physics G: Nuclear and Particle Physics

PAPER

Anisotropy of low energy direct photons in relativistic heavy ion collisions

To cite this article: T Koide and T Kodama 2016 *J. Phys. G: Nucl. Part. Phys.* **43** 095103

IOP Publishing Journal of Physics G: Nuclear and Particle Physics

J. Phys. G: Nucl. Part. Phys. **43** (2016) 095103 (12pp) doi:10.1088/0954-3899/43/9/095103

Anisotropy of low energy direct photons in relativistic heavy ion collisions

T Koide[1] **and T Kodama**

Instituto de Física, Universidade Federal do Rio de Janeiro, C.P. 68528, 21941-972, Rio de Janeiro, Brazil

E-mail: tomoikoide@gmail.com

Received 20 May 2016, revised 7 July 2016
Accepted for publication 19 July 2016
Published 10 August 2016

CrossMark

Abstract

Using the Wigner function approach for electromagnetic radiation fields, we investigate the behavior of low energy photons radiated by the deceleration processes of two colliding nuclei in relativistic heavy ion collisions. The angular distribution reveals information of the initial geometric configurations, which is reflected in the anisotropic parameter v_2, with an increasing v_2 as energy decreases. This behavior is qualitatively different to the v_2 from the hadrons produced in the collisions.

Keywords: relativistic heavy ion collisions, photon, elliptic flow

1. Introduction

In the physics of relativistic heavy ion collisions, the determination of the initial collision geometry is one of the fundamental pieces of information required to investigate the dynamics of the created matter, such as quark–gluon plasma. Knowledge of the reaction plane is indispensable to study the anisotropic collective flows of the matter. This geometry is deduced indirectly from, for example, the statistical average over an event ensemble by calculating the cumulant of the correlation functions of hadrons, which are generated through very complex strong interactions [1]. On the other hand, photons do not suffer from strong interactions, and the so-called direct photons are considered to carry information about the early stages of collisions. Numerous studies in this line have been carried out from the early days of the relativistic heavy ion program [2–18]. See [19] for a recent review on this subject and also the references therein.

Among the various mechanisms for producing direct photons, we consider bremsstrahlung radiation. This process is usually modeled as classical radiation from the decelerated protons of the incident nuclei [2–11]. In [20], the authors focused on the behavior of the

[1] Author to whom any correspondence should be addressed.

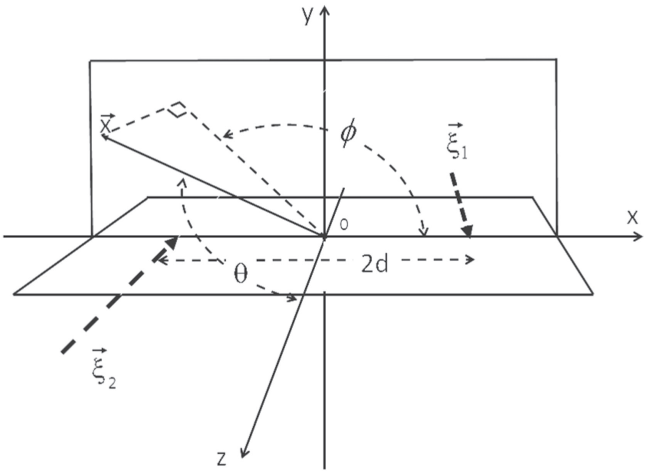

Figure 1. The schematic for the collision of two incident nuclei.

higher energy ($\gtrsim$1 GeV) photons, which are dominantly produced by the incoherent sum of the bremsstrahlung radiation from individual decelerated protons, reproducing the spectrum of the observed radiation [21]. In this case, any meaningful information on the initial geometry on the nuclear scale is expected to be washed out.

However, for lower energies electromagnetic fields may be generated *coherently* from each decelerating proton, when their spatial separation is on the order of the corresponding wavelength of the radiation. If this occurs, we expect the following two effects. The first is that the amount of radiation increases as $\sim Z_{\rm eff}^2$, instead of $2Z_{\rm eff}$ in the incoherent case, where $Z_{\rm eff}$ is the effective number of charges which contribute to the electromagnetic radiation in the collisions. The second is that the angular distribution of the radiated photons will reflect the geometric configuration due to the interference of radiation from the two incident nuclei. When we have a sufficient yield of coherent photons in the very low transverse momentum p_T region, the elliptic flow v_2 for the direct photons will be dominated by such coherent photons.

In this work, we study the photon spectrum and its angular distributions of the low energy photons, which are produced by the coherent radiation from two decelerated incident nuclei. We first calculate the electromagnetic fields by introducing the simplified trajectories of the two incident nuclei. These nuclei are treated as point-like objects with an effective charge $Z_{\rm eff}$. From this, we obtain the phase-space distribution of the photons with the help of the Wigner function, which expresses the photon spectrum and the angular distribution. We further show that the corresponding anisotropic parameter v_2 reveals a very enhanced nature in the lower $p_{\rm T}$.

In the following, we use $\hbar = c = \varepsilon_0 = \mu_0 = 1$ and the fine structure constant is defined by $\alpha_{\rm EM} = e^2/(4\pi)$ in the SI (rationalized) unit.

2. Model of collisions and electromagnetic radiation

Let us consider a collision of two identical nuclei with the impact parameter b . In the strong coherence limit, we can simplify the situation by replacing these nuclei with point-like particles which have an effective charge $Z_{\rm eff}$. One may expect that $Z_{\rm eff}$ is the same as the number of participant protons $Z_{\rm part}(b)$ from one of the nuclei, but more generally, only a portion of the participant protons can contribute to the coherent radiation. Then we have the restriction,

$Z_{\rm eff} \lesssim Z_{\rm part}(b)$. We further consider that the protons in each nucleus will be completely stopped by the collisions with other protons or neutrons, as is the initial condition of the Landau hydrodynamic model. Our geometrical coordinate is represented in figure 1, where the $z-$axis is chosen as the collision direction and the two incident nuclei collide at $t = 0$.

In general, the deceleration by the collisions occurs in a finite time period, which is characterized by stopping time τ_S. For the ultra-relativistic heavy ion collisions, τ_S is given by the order of the Lorentz contracted thickness of the projectile, $\tau_S \sim R/\gamma$, where R and γ are the nuclear radius and the Lorentz factor, respectively. For the relativistic limit $\gamma \gg 1$ the stopping time will be very small. For the sake of simplicity, we consider the infinitesimal limit of τ_S. In this case, the deceleration is given by the Dirac delta function in time. See also the discussion in appendix A.

Then the trajectories of the nuclei 1 and 2 are, respectively, expressed in the Cartesian coordinates as

$$\vec{\xi}_1(t) = \begin{pmatrix} d \\ 0 \\ t\ V_0\ \theta(-t) \end{pmatrix},\ \vec{\xi}_2(t) = \begin{pmatrix} -d \\ 0 \\ -t\ V_0 \theta(-t), \end{pmatrix}, \tag{1}$$

where $2d$ represents the transverse distance between the two centers of mass of the respective participant protons (see figure 1). This is usually smaller than the impact parameter, $2d \lesssim b$. At infinite distance ($t = -\infty$), the nuclei move with a constant speed V_0 which should be less than one.

The solution of the Maxwell equations for these trajectories is given by the Liénard–Wiechert potential [22]. Since we are interested in the behaviors of the radiation at the detector position, we drop irrelevant contributions at infinite distance. Then, the contributions from the charge $\vec{\xi}_1(t)$ are given by

$$\begin{aligned} \vec{E}_1(\vec{x},\, t) &= \frac{eV_0 Z_{\rm eff}}{4\pi} \frac{1}{|\vec{x} - \vec{\xi}_1(t_1)|} \frac{1}{1 - \vec{\beta}_1 \cdot \vec{n}_1} \\ &\times \{(1 - \vec{n}_1 \vec{n}_1^T)\vec{e}_z\}\,\delta(t_1), \\ \vec{B}_1(\vec{x},\, t) &= \vec{n}_1 \times \vec{E}_1(\vec{x},\, t) \end{aligned}$$

where $\vec{e}_z$ is a unit vector parallel to the $z-$axis and

$$\vec{n}_1 \equiv \frac{\vec{x} - \vec{\xi}_1(t_1)}{|\vec{x} - \vec{\xi}_1(t_1)|}, \qquad \vec{\beta}_1 \equiv \left.\frac{d\vec{\xi}_1}{dt}\right|_{t=t_1}$$

All the quantities appearing on the right-hand sides are evaluated at the emission time t_1, defined by the causality equation, $|\vec{x} - \vec{\xi}_1(t_1)| = t - t_1$.

Therefore, eliminating the emission times, $\vec{E}_1(\vec{x},\, t)$ and $\vec{B}_1(\vec{x},\, t)$ are re-expressed as

$$\vec{E}_1(\vec{x},\, t) = \frac{eV_0 Z_{\rm eff}}{4\pi} \frac{1}{r_-^3} \begin{pmatrix} -(x-d)z \\ -yz \\ (x-d)^2 + y^2 \end{pmatrix} \delta(t - r_-), \tag{2a}$$

$$\vec{B}_1(\vec{x},\, t) = \frac{eV_0 Z_{\rm eff}}{4\pi} \frac{1}{r_-^2} \begin{pmatrix} y \\ -(x-d) \\ 0 \end{pmatrix} \delta(t - r_-), \tag{2b}$$

where $r_- = \sqrt{(x-d)^2 + y^2 + z^2}$. The corresponding electromagnetic fields from $\vec{\xi}_2(t)$ can be obtained by replacing the two parameters $(d,\, V_0)$ by $(-d,\, -V_0)$ in equation (2).

3. The Wigner function of electromagnetic fields

To extract the spectrum of the photons radiated from the classical electromagnetic fields, the frequency distribution of the radiation energy is often interpreted as the energy distribution of photons with the help of Einstein's relation. However, it is known that the classical electromagnetic field can be interpreted as the wave function of the corresponding photons [23–26]. Here we employ this approach to calculate the photon angular distribution.

Let us introduce a complex vector function as

$$\vec{F} = \sqrt{\frac{1}{2}}(\vec{E} + \mathrm{i}\vec{B}). \tag{3}$$

Then the source-free Maxwell's equations can be re-expressed in a similar form to the Dirac equation as

$$\mathrm{i}\partial_t \vec{F} = -\mathrm{i}(\vec{T} \cdot \nabla)\vec{F}, \tag{4}$$

with a constraint,

$$\nabla \cdot \vec{F} = 0, \tag{5}$$

where $\vec{T}$ is the spin-1 generator of $O(3)$. Equation (5) constrains only the initial condition of $\vec{F}$. From the definition, one can easily see that the energy density and the Poynting vector are expressed as $\vec{F}^* \cdot \vec{F}$ and $-\mathrm{i}\,\vec{F}^* \times \vec{F}$, respectively. For other properties of this quantum-mechanical interpretation of the vector wave function see [25].

To discuss the physical observables measured by a detector at a given location, it is convenient to introduce the phase-space distribution function, known as the Wigner function. In the present case, we have

$$\begin{aligned} f_{\mathrm{W}}(\vec{x}, \vec{p}, t) &\equiv \int \mathrm{d}^3\vec{q}\,\vec{F}^*(\vec{x} + \vec{q}/2, t) \cdot \vec{F}(\vec{x} - \vec{q}/2, t)\mathrm{e}^{\mathrm{i}\vec{q}\cdot\vec{p}} \\ &= f_{\mathrm{W}}^{(E)}(\vec{x}, \vec{p}, t) + f_{\mathrm{W}}^{(B)}(\vec{x}, \vec{p}, t), \end{aligned}$$

where $f_{\mathrm{W}}^{(E,B)}$ represents the contribution from the electric (magnetic) field. After some algebra, we find

$$\begin{aligned} f_{\mathrm{W}}^{(E,B)}(\vec{x}, \vec{p}, t) = &\, G^{(E,B)}(\vec{x} - \vec{d}, \vec{p}; t) + G^{(E,B)}(\vec{x} + \vec{d}, \vec{p}; t) \\ &- 2\cos(2\vec{p} \cdot \vec{d})G^{(E,B)}(\vec{x}, \vec{p}; t), \end{aligned} \tag{6}$$

$$G^{(E,B)}(\vec{x}, \vec{p}; t) \equiv \int \mathrm{d}^3\vec{q} \times \{\vec{F}^{(E,B)}(\vec{x} + \vec{q}/2, t) \cdot \vec{F}^{(E,B)}(\vec{x} - \vec{q}/2, t)\}\mathrm{e}^{\mathrm{i}\vec{q}\cdot\vec{p}}, \tag{7}$$

and

$$\vec{F}^{(E)}(\vec{x}, t) \equiv \sqrt{\frac{1}{2}}\frac{eV_0 Z_{\mathrm{eff}}}{4\pi}\frac{1}{r^3}\begin{pmatrix} -xz \\ -yz \\ x^2 + y^2 \end{pmatrix}\delta(t - r),$$

$$\vec{F}^{(B)}(\vec{x}, t) \equiv \sqrt{\frac{1}{2}}\frac{eV_0 Z_{\mathrm{eff}}}{4\pi}\frac{1}{r^2}\begin{pmatrix} y \\ -x \\ 0 \end{pmatrix}\delta(t - r).$$

Here, $r = |\vec{x}|$ and $\vec{d} = (d, 0, 0)$.

As is well-known, the Wigner function does not correspond to the phase-space distribution since, in general cases, it can take negative values. However, as shown below, the large distance behavior guarantees the non-negativity of the Wigner function. Since $\vec{x}$ and t

are macroscopic quantities associated with the physical measurements of a detector, they are much larger than the magnitude of $1/p$, where p is on the order of MeV~GeV. Thus, the significant contributions in the q integrals in equation (7) come from the domain satisfying $q \ll r,\, t$ due to the exponential factor in the integrands. Therefore we can safely expand them with respect to q/r. The integrands contain the product of two delta functions with respect to t, which is approximately re-expressed as $\delta(t - \sqrt{(\vec{x} + \vec{q}/2)^2})\ \delta(t - \sqrt{(\vec{x} - \vec{q}/2)^2}) \simeq \delta(t - r)\delta(q_{\|})$, where $q_{\|}$ is the component of $\vec{q}$ parallel to $\vec{x}$. Then we have

$$\begin{aligned} G^{(E)}(\vec{x}, \vec{p}, t) &= C(\vec{x})\delta(t - r)\int \mathrm{d}^2\mathbf{q}_\perp \mathrm{e}^{\mathrm{i}\mathbf{p}_\perp\cdot\mathbf{q}_\perp} + O\left(\frac{1}{r^3}\right) \\ &\simeq (2\pi)^2 C(\vec{x})\delta(t - r)\delta^{(2)}(\vec{p}_\perp), \end{aligned}$$

where $\vec{p}_\perp$ is the orthogonal component of $\vec{p}$ to $\vec{x}$, and

$$C(\vec{x}) = \frac{\alpha_{\mathrm{EM}}}{8\pi}(V_0 Z_{\mathrm{eff}})^2 \frac{1}{r^2}\sin^2\theta.$$

In the above, θ is the azimuthal angle of $\vec{x}$ with respect to the z-axis (see figure 1). For $r \gg d$, we find

$$G^{(E)}(\vec{x}, \vec{p}, t) \simeq G^{(B)}(\vec{x}, \vec{p}, t),$$

and

$$G^{(E,B)}(\vec{x}, \vec{p}, t) \simeq G^{(E,B)}(\vec{x} + \vec{d}, \vec{p}, t) \simeq G^{(E,B)}(\vec{x} - \vec{d}, \vec{p}, t).$$

Then the Wigner function is finally expressed as

$$\begin{aligned} f_{\mathrm{W}}(\vec{x}, \vec{p}, t) \simeq{}& 4(2\pi)^2 C(\vec{x})\{1 - \cos(\vec{p}\cdot\vec{d})\}\delta(t - r) \\ &\times 2\frac{1}{p^2}\delta^{(2)}(\Omega_{\vec{p}} - \Omega_{\vec{x}}), \end{aligned} \tag{8}$$

where $\Omega_{\vec{p}}$ and $\Omega_{\vec{x}}$ are the solid angles for $\vec{p}$ and $\vec{x}$, respectively. The factor 2 in the last term of the above equation comes from the two opposite directions contained in $\delta^{(2)}(\vec{p}_\perp)$. Equation (8) clearly shows that $f_{\mathrm{W}}(\vec{x}, \vec{p}, t)$ is positive semi-definite.

From this Wigner function, the energy distributions in the $\vec{x}$ and $\vec{p}$ spaces are given by

$$\frac{\mathrm{d}^3\mathcal{E}}{\mathrm{d}\vec{x}^3} = \frac{1}{(2\pi)^3}\int \mathrm{d}^3\vec{p}\ f_{\mathrm{W}}(\vec{x}, \vec{p}, t), \tag{9}$$

and

$$\frac{\mathrm{d}^3\mathcal{E}}{\mathrm{d}\vec{p}^3} = \frac{1}{(2\pi)^3}\int \mathrm{d}^3\vec{x}\ f_{\mathrm{W}}(\vec{x}, \vec{p}, t), \tag{10}$$

respectively.

4. Photon spectrum

Substituting equation (8) into equation (10), we obtain the momentum spectrum. Because of the Dirac delta functions in equation (8), note that this is equivalent to the sum of all energies of the incoming photons to a detector at $\vec{R}_D$,

$$\frac{\mathrm{d}^3\mathcal{E}}{\mathrm{d}\vec{p}^3} = \frac{1}{(2\pi)^3}\int \mathrm{d}t \int_{\vec{\Omega}\in D} \mathrm{d}^2\vec{\Omega}_{\vec{R}_D} R_D^2\, f_{\mathrm{W}}(\vec{R}_D, \vec{p}, t), \tag{11}$$

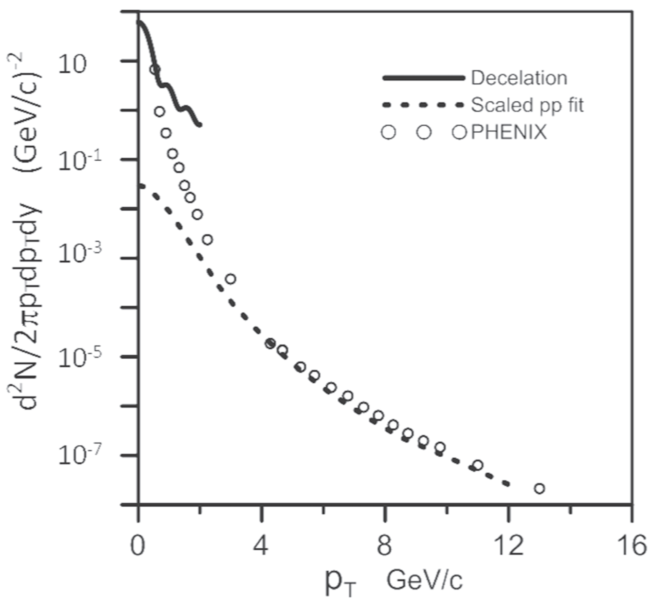

Figure 2. The photon spectrum. The solid line represents the results from our model calculation. The circles and dashed line indicate the PHENIX data [21] and the scaled proton–proton collision fit, respectively.

where the integral for the solid angle $\vec{\Omega}_{\vec{R}_D}$ is performed within the domain D corresponding to the aperture of the detector. In the above, we integrate all photon energies coming into the detector. Re-expressing this with the photon number N, we have

$$\frac{d^3N}{d\vec{p}_T^2 dy} = \frac{1}{2\pi^2} \frac{\alpha_{EM}(V_0 Z_{eff})^2}{p^2 \cosh^2 y} \{1 - \cos(2\vec{p} \cdot \vec{d})\}, \tag{12}$$

where y represents the rapidity. See appendix B. In the following calculations, we choose $V_0 = 1$.

For example, let us take $Z_{eff} \sim 80$ and $d \sim 1$ fm as a near central Au + Au collisions. In this case, the order of the magnitude of the photon spectrum is

$$\left.\frac{d^3N(p)}{2\pi p_T d_{pT} dy}\right|_{y=0} \simeq 0.37 \times 10^{-3} \frac{Z_{eff}^2}{p_T^2}(1 - J_0(2p_T d)), \tag{13}$$

where J_n is the Bessel function of order n. In figure 2, we show the behavior of the above rough estimate (solid line) together with the PHENIX data, just for the sake of comparison. Although our calculation seems to be consistent with the experimental data, our idealization of full stopping is not well satisfied in RHIC energies. Rather, our model will be more suitable for experiments on the lower energies such as the NICA or FAIR programs [27, 28], where a large stopping power is expected. Note that if we calculate the same spectrum assuming incoherent radiation as is done in [20], the magnitude of the spectrum decreases by one or two orders.

The angular distribution of the photons reveals an interesting behavior as shown in figure 3. Here, we plotted only the factor $1 - \cos(2\vec{p} \cdot \vec{d})$ in the radial coordinate with respect to the azimuthal angle ϕ at the vanishing rapidity $y = 0$ where $p = p_T$, and we find

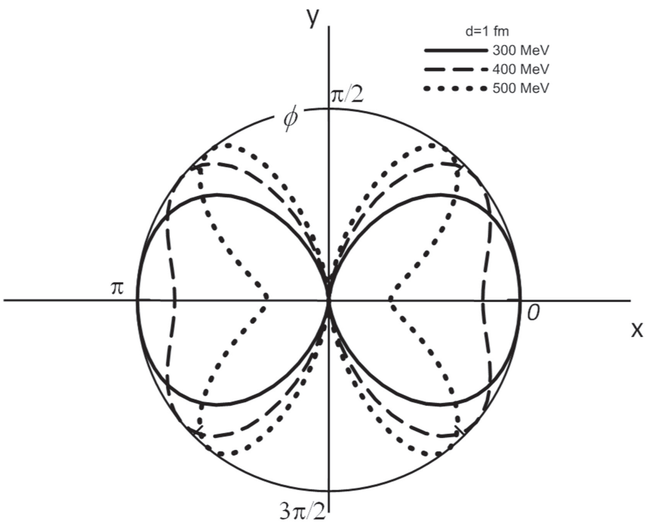

Figure 3. The angular distributions at $y = 0$. The solid, dashed, and dotted lines represent the results of $p_T = 300$, 400, and 500 MeV, respectively. The axes x and y correspond to those in figure 1.

that there are common dips at $\phi = \pm\pi/2$. These dips correspond to the direction of the normal vector to the reaction plane. If such a feature is measurable experimentally, we could determine the event plane unmistakably and even determine the parameter d quantitatively.

However, unfortunately, the total yield of such low energy photons is very small (<20) even in the most favorable conditions of our model. If we consider the further experimental difficulties in the detection of the low energy photons, the determination of the event geometry in the event-by-event (EbyE) basis seems to be unrealistic.

On the other hand, the above peculiar behavior will be reflected in another tractable observable, the anisotropic parameter, such as v_2. In our model, v_2 is calculated as

$$v_2(p_T) = \frac{J_2(2p_T d)}{1 - J_0(2p_T d)}. \tag{14}$$

A similar expression was calculated by [29] in a different context. In figure 4, we plot the above v_2 for $d = 1$ fm as before. In contrast to the well-known behavior of v_2, the coherent electromagnetic radiation shows an increasing v_2 for the lower p_T, achieving its maximum value $1/2$ for $p_T \to 0$, independent of the value of d. Therefore, if such an increase of v_2 in the low energy photons ($p_T < 0.5$ GeV) is found experimentally, it can be considered as a genuine signal from the coherent electromagnetic radiation of the deceleration, although it will be affected by the incoherent radiation. See the discussion in section 5. Such a behavior is not expected from the usual hydrodynamic, kinetic, or microscopic pictures of the collective flow mechanism [19, 30].

5. Concluding remarks and discussion

In this short exercise, we investigated the behavior of the low energy photons radiated by the deceleration processes of the two incident nuclei in relativistic heavy ion collisions. We assumed that the coherent radiation is dominant, so that the two colliding nuclei are replaced

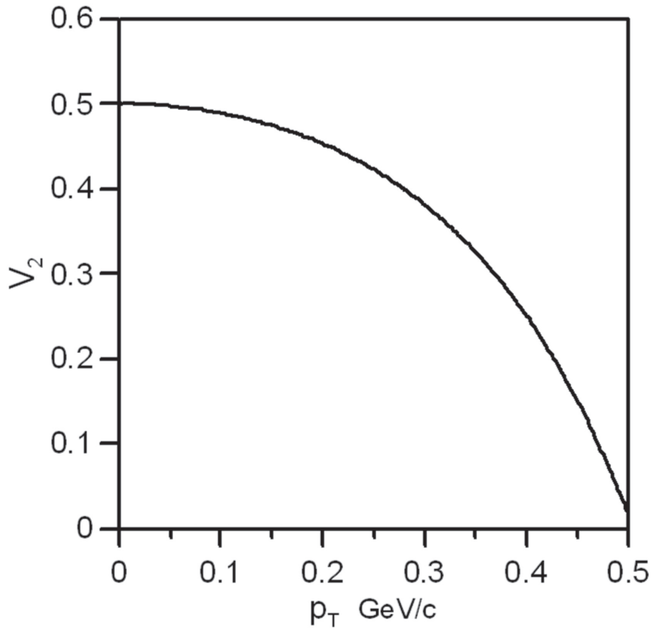

Figure 4. Low energy behavior of v_2 of the direct photons obtained from the coherent radiation for $d = 1$ fm.

by point charges, and the deceleration mechanism is simply characterized by the Dirac delta function. We thus consider a full stopping scenario, such as the Landau-type initial condition, which may have better prospects in lower energy heavy ion collisions, such as the upcoming NICA and FAIR experiments [27, 28].

We found that the angular distribution of the low energy photons reveals well the initial geometric configurations at the deceleration processes. Such a property is reflected in the anisotropic parameter v_2, showing a very enhanced nature in the lower p_T. If the angular distribution is measurable in the EbyE basis, the initial geometry could be determined. However, the total photon multiplicity in our model is on the order of 10~20 in an optimistic situation, so that the EbyE based analysis seems to be improbable. On the other hand, since these signals have characteristic patterns for a given initial geometry, they may be still useful to improve the determination of the initial conditions by using, for example, their correlations with other particles. Another interesting possibility for the multiple soft photon emission mechanism was suggested in [31], but the nature of the angular distribution of the produced photons would be different from ours.

In this work, we considered a very idealized model of the deceleration where the coherent electromagnetic radiation occurs from the overall nuclear charges, and did not discuss a mechanism to maintain such a coherence by relativistic heavy ion collisions. To clarify these points and examine the above possibilities, it is important to apply the present approach to more realistic initial conditions and possible collective deceleration mechanisms, for example, shock wave formation [11]. The Wigner function approach described here will be useful for this purpose. We leave this as a future task.

As shown in figure 4, our coherent radiation of the low energy photons exhibits an increasing v_2 as energy decreases, achieving its maximum value $1/2$ at $p_T = 0$. This is the case considering only the coherent radiation. As discussed, the coherence for higher momenta

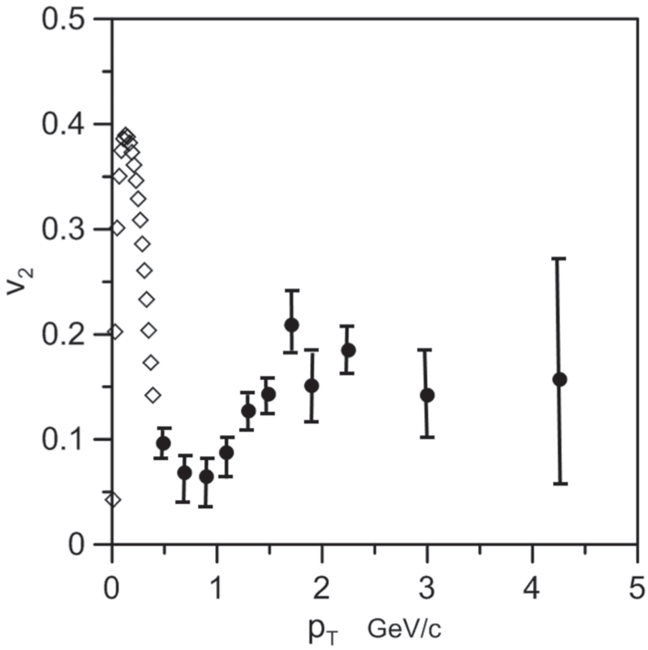

Figure 5. v_2 from direct photons. Squares denote the results with the effects of the incoherent mechanism given by equation (15) with $\Delta p = 0.2$ GeV. Filled circles indicate the experimental data from PHENIX [21].

will be quickly destroyed and incoherent photons should be dominant. We may roughly evaluate such an effect assuming that the coherent contribution vanishes exponentially with a characteristic scale Δp as a function of p_T, while the incoherent contribution becomes dominant for $p_T \gg \Delta p$. In such a case, the anisotropic parameter v_2 in equation (14) is replaced by

$$v_2(p_T) = \frac{J_2(2p_T d)}{1 + 2e^{2p_T/\Delta p}/Z_{\text{eff}} - J_0(2p_T d)}. \tag{15}$$

In figure 5, we show the results of equation (15) for $\Delta p = 0.2$ GeV with squares. For the sake of comparison, the PHENIX data are also plotted (filled circles) [21]. Note that in the presence of the incoherent contribution, v_2 vanishes at $p_T = 0$ and the maximum is shifted to a finite value of p_T. Current experimental measurements of v_2 of the direct photons are only from 0.5 GeV and above [21], and thus it is still difficult to see whether the coherent radiation mechanism is present or not. However, it is interesting to note that the experimental data seem to show the beginning of such an increase for $p_T \leqslant 0.5$ GeV as is shown in figure 5, which is qualitatively in agreement with the behavior of v_2 calculated with the coherent radiation mechanism. Of course, our deceleration scenario is not applicable to the RHIC experiment, so any direct comparison will not be appropriate. On the other hand, if this behavior of v_2 is attributed to the coherent radiation of the photons, we expect that such a signature should be enhanced in NICA and FAIR. In this aspect, the measurements of the lower energy direct photons are essential to clarify the presence of the coherent mechanism in relativistic heavy ion collisions.

Acknowledgments

The authors acknowledge E L Bratkovskaya, G S Denicol, M Greif, and C Greiner for useful discussions and comments. We also thank E Kokoulina for calling our attention to [31]. This work is financially supported by CNPq and CAPES.

Appendix A. Sensitivity of the rapidity distribution on deceleration

The trajectories (1) can be considered as if we take the vanishing τ_S limit of the parameterization of a continuous deceleration,

$$\vec{\xi}_1(t) = \begin{pmatrix} d \\ 0 \\ t \ \ V_0 \ \tanh\left(\frac{t}{\tau_S}\right) \theta(-t) \end{pmatrix}, \tag{A1}$$

$$\vec{\xi}_2(t) = \begin{pmatrix} -d \\ 0 \\ -t \ \ V_0 \ \tanh\left(\frac{t}{\tau_S}\right) \theta(-t), \end{pmatrix}, \tag{A2}$$

which is similar to [20], except for the difference in the argument of tanh.

Substituting this into the above calculations and taking the vanishing limit of τ_S, we find that the factor $\{1 - \cos(2\vec{p} \cdot \vec{d})\}/p^2$ in equation (12) is replaced by

$$\frac{1}{2p^2}\left\{\frac{1}{(1 - V_0 \tanh y)^2} + \frac{1}{(1 + V_0 \tanh y)^2} - 2\frac{1}{1 - V_0^2 \tanh^2 y}\cos(2\vec{p} \cdot \vec{d})\right\}. \tag{A3}$$

In particular, in the ultra-relativistic limit ($V_0 \to 1$), the angular distribution of the photons is given by

$$\frac{\mathrm{d}^3 N}{\mathrm{d}\vec{p}_T^2 \mathrm{d}y} = \frac{1}{2\pi^2}\frac{\alpha_{EM}(V_0 Z_{\mathrm{eff}})^2}{p^2}\{\cosh(4y) - \cos(2\vec{p} \cdot \vec{d})\}. \tag{A4}$$

One can see that the rapidity distribution shows a rather hyperbolic increase for $|y| \gg 1$, so that the photon yield is strongly enhanced in the forward and backward directions, while the angular distribution tends to be isotropic. However, for the central rapidity $y = 0$, the above result still coincides with equation (12). Therefore, in the plane at the central rapidity, the angular distribution of photons is independent of the deceleration mechanism as long as the time scale τ_S is small enough. This suggests the possibility that the behavior at $y = 0$ is relatively insensitive to deceleration mechanisms if the characteristic time scale of the deceleration is small enough .

For the sake of comparison, let us consider the incoherent limit. Then our spectrum for the deceleration of the Dirac delta function, equation (12), is replaced by

$$\frac{\mathrm{d}^3 N}{\mathrm{d}\vec{p}_T^2 \mathrm{d}y} = \frac{1}{2\pi^2}\alpha_{EM} V_0^2 Z_{\mathrm{eff}} \frac{1}{p^2 \cosh^2 y}. \tag{A5}$$

On the other hand, in the small τ_S limit of the continuous deceleration, equation (A4), we have

$$\frac{\mathrm{d}^3 N}{\mathrm{d}\vec{p}_T^2 \mathrm{d}y} = \frac{1}{2\pi^2}\alpha_{EM} V_0^2 Z_{\mathrm{eff}} \frac{1}{p^2}\cosh(4y). \tag{A6}$$

These rapidity dependencies are, respectively, to be compared with the low energy limit and the Rindler acceleration cases discussed in [20]. However, in our case, equation (A5) does not necessarily correspond to the non-relativistic case, since V_0 can be arbitrary close to unity, and equation (A6) shows a faster increase in rapidity compared to the large deceleration limit of the Rindler case. That is, the difference of the deceleration mechanism drastically changes the rapidity distribution of the photons. See also the related calculations in [32].

Appendix B. Rapidity

Our variables, shown in figure 1, can be expressed in terms of the rapidity. For the sake of simplicity, we consider the case where the mass is negligibly small. Then the rapidity is defined by

$$y = \frac{1}{2} \ln \frac{p + p_z}{p - p_z}. \tag{B1}$$

Then the energy and longitudinal momentum are expressed as

$$p = p_T \cosh y, \tag{B2}$$

$$p_z = p_T \sinh y. \tag{B3}$$

We can also express p_z as

$$\cos\theta = \frac{p_z}{p}. \tag{B4}$$

Substituting this into equation (B1), we have

$$\cos\theta = \tanh y, \tag{B5}$$

$$\sin\theta = \frac{1}{\cosh y}. \tag{B6}$$

References

[1] See, for example Derradi de Souza R, Koide T and Kodama T 2016 *Prog. Part. Nucl. Phys.* **86** 35
[2] Kapsta J 1977 *Phys. Rev.* C **15** 1580
[3] Bjorken J D and McLerran L 1985 *Phys. Rev.* D **31** 63
[4] Thiel J *et al* 1989 *Nucl. Phys.* A **504** 864
[5] Koch V *et al* 1990 *Phys. Lett.* B **236** 135
[6] Lippert T *et al* 1991 *Int. J. Mod. Phys.* A **29** 5249
[7] Dumitru A *et al* 1993 *Phys. Lett.* B **318** 583
[8] Eichmann U and Greiner W 1997 *J. Phys.* G **23** L65
[9] Jeon S *et al* 1998 *Phys. Rev.* C **58** 1666
[10] Kapusta J and Wong S M H 1999 *Phys. Rev.* C **59** 3317
[11] Eichmann U *et al* 2000 *Phys. Rev.* C **62** 044902
[12] Ruuskanen P A 1992 *Nucl. Phys.* A **544** 169c-182c
[13] Chatterjee R *et al* 2011 *Phys. Rev.* C **83** 054908
[14] Chaudhuri A K and Sinha B 2011 *Phys. Rev.* C **83** 034905
[15] Shen C *et al* 2015 *Phys. Rev.* C **91** 024908
[16] Gale C *et al* 2015 *Phys. Rev. Lett.* **114** 072301
[17] Endres S *et al* 2015 *Phys. Rev.* C **92** 014911
[18] Alam J, Raha S and Sinha B 1996 *Phys. Rep.* **273** 243

[19] Linnyk O, Bratkovskaya E L and Cassing W 2016 *Prog. Part. Nucl. Phys.* **87** 50
[20] Biró T S, Gyulassy M and Schram Z 2012 *Phys. Lett.* B **708** 276
[21] PHENIX collaboration 2015 arXiv:1509.07758
[22] Jackson J D 1999 *Classical Electrodynamics* 3rd edn (New York: Wiley)
[23] Silberstein L 1907 *Ann. d. Ohys.* **22** 579
Silberstein L 1907 *Ann. d. Ohys.* **24** 783
[24] Bateman H 1915 *The Mathematical Analysis of Electrical and Optical Wave Motion on the Basis of Maxwell's Equations* (Cambridge: Cambridge University Press)
[25] Bialynicki-Birula I 1994 *Act. Phys. Pol.* A **86** 97
[26] Holland P 2005 *Proc. R. Soc.* A **461** 359
[27] Höhne C 2013 *J. Phys.: Conf. Ser.* **420** 012016
[28] Schmidt H R 2014 *J. Phys.: Conf. Ser.* **509** 012084
[29] Biró T S, Horváth M and Schram Zs 2015 *Eur. Phys J.* A **51** 75
[30] Paquet J-F *et al* 2016 *Phys. Rev.* C **93** 044906
[31] Lichard P and Hove L Van 1999 *Phys. Lett.* B **245** 605
[32] Biró T S, Szendi Z and Schram Z 2014 *Euro. Phys. J.* A **50** 62